

Journal Pre-proof

A spectral pedestrian-based approach for modal identification

André Jesus, Stana Živanović, Amir Alani

PII: S0022-460X(19)30720-5

DOI: <https://doi.org/10.1016/j.jsv.2019.115157>

Reference: YJSVI 115157

To appear in: *Journal of Sound and Vibration*

Received Date: 29 April 2019

Revised Date: 11 December 2019

Accepted Date: 13 December 2019

Please cite this article as: André. Jesus, S. Živanović, A. Alani, A spectral pedestrian-based approach for modal identification, *Journal of Sound and Vibration* (2020), doi: <https://doi.org/10.1016/j.jsv.2019.115157>.

This is a PDF file of an article that has undergone enhancements after acceptance, such as the addition of a cover page and metadata, and formatting for readability, but it is not yet the definitive version of record. This version will undergo additional copyediting, typesetting and review before it is published in its final form, but we are providing this version to give early visibility of the article. Please note that, during the production process, errors may be discovered which could affect the content, and all legal disclaimers that apply to the journal pertain.

© 2019 Published by Elsevier Ltd.



A Spectral Pedestrian-based Approach for Modal Identification

André Jesus^{a,*}, Stana Živanović^b, Amir Alani^c

^a*Faculty of Environment and Technology, University of the West of England, Coldharbour Lane, Frenchay Campus, Bristol BS16 1QY, UK*

^b*College of Engineering, Mathematics and Physical Sciences, University of Exeter, Exeter EX4 4QF, UK*

^c*School of Computing and Engineering, University of West London, St. Mary's Road, Ealing, London, W5 5RF, UK*

Abstract

The dynamic behaviour of footbridges is characterised by modal properties such as natural frequencies, mode shapes, damping ratios and modal masses. Their estimation via modal tests often requires expensive or difficult-to-operate equipment (e.g. shaker and instrumented impact hammer) or, sometimes unavailable high signal-to-noise ratios in tests relying on natural (e.g. wind, airborne noise and ground-borne vibration) excitation. In addition, the modal properties determined in modal tests do not necessarily apply to the structure under pedestrian traffic in case of amplitude-dependent frequencies and damping ratios. The current work proposes a novel approach that stands in contrast to the widely used tests, based on modal identification using an excitation induced by a single pedestrian. In order to account for estimation and observation uncertainties, the relationship between the power spectrum of the response and its modal properties is described with a likelihood function. It is shown that it is possible to reliably estimate modal properties using pedestrian walk forces measured in the laboratory, and dynamic responses measured when the same pedestrian is crossing a footbridge at timed pacing rates. The approach is validated using numerical and field data for a 16.9 m long fibre reinforced polymer footbridge.

*Corresponding author

Email address: andrejhjesus@gmail.com (André Jesus)

This work paves a new way for simple and low cost modal testing in structural dynamics.

Keywords: power spectral density, modal identification, FRP footbridge, pedestrian excitation, Metropolis–Hastings, likelihood function.

1. Introduction

2 Structural assessment via modal testing is a vast area of research, enabled
 by advanced signal processing techniques and excitation methods [1]. The se-
 4 lected approach is often based on operational constraints, such as time, cost-
 effectiveness, ease-of-use, type of structure and available excitation.

6 Flexible large-scale structures are usually best tested using ambient exci-
 tation. Data analysis employs methods that are developed assuming that vi-
 8 brations are random (i.e. broadband) and that signal-to-noise ratio (SNR) is
 high. Much progress has been made in the processing techniques that utilise
 10 these types of measurements [2–5]. For medium-scale structures, the most sig-
 nificant modes of vibration might be excitable with more controllable sources:
 12 such as instrumented moving vehicles [6], or with medium/high-force shakers.
 Finally for structures such as footbridges, the main equipment for excitation are
 14 portable shakers and hand-held impact hammers, although ambient testing is
 occasionally used as well.

16 Both shakers and impact hammers have their drawbacks. With a shaker,
 the frequency response function (FRF) is constructed from the excitation signal
 18 (such as sweep sine, chirp, or random excitation) and simultaneously measured
 vibration responses. This type of test is very reliable, but it is expensive and
 20 might be difficult to execute in difficult-to-access sites due to heavy weight of
 the shaker (often more than 50 kg). Hammer impact testing drawbacks are poor
 22 SNR, high sensitivity to non-linearities and a lack of control over the frequency
 content of the excitation. Concerning cost-effectiveness of these two solutions,
 24 the impact hammer provides the more economic option, that could be about ten
 times less expensive than testing with the shaker [7]. Ambient test is similarly

26 affordable, but could suffer from low SNR.

In all these tests the identification of natural frequencies is the most reliable
 28 and modal masses are the most difficult (or even impossible in the ambient test-
 ing) to identify. It is not uncommon to see errors in the order of 1 % for natural
 30 frequencies and 30 % for damping ratios and modal masses—as illustrated in
 Section 18.5.3 of [8] and Chapter 1 of [9]. As a consequence, some have instead
 32 tried to estimate modal masses with human tests, as proposed by Brownjohn
 and Pavic [10]. Such tests are attractive since they are cost-effective, easy and
 34 quick to perform. In addition, Brownjohn and his co-workers [11] used human
 excitation generated whilst jumping and measured using either a force plate or
 36 inertial measurement units. They also measured acceleration response of the
 structure to estimate the frequency response function (FRF) of one vibration
 38 mode at a time. It should be noted that nearly all examples of this body of
 research relied solely on jumping tests to identify properties of individual vi-
 40 bration modes. Probabilistic models were seldom used despite of the inherent
 uncertainties [12–14].

42 This work investigates the applicability of a modal identification approach
 using the dynamic excitation by a pedestrian. In contrast to the previous re-
 44 search, the proposed approach can be used for simultaneous identification of
 multiple vibration modes, and it accounts for estimation and observation uncer-
 46 tainties using a likelihood function of the “bridge-pedestrian” spectral response.
 The identification process requires two main inputs: recordings at a range of
 48 pacing rates of structural responses under passage of a given pedestrian; and the
 pedestrian-induced dynamic forces (measured on, say, an instrumented treadmill
 50 in a laboratory at the same pacing rates). Validation is illustrated with both
 simulated and field data from a 16.9 m long fibre reinforced polymer (FRP)
 52 footbridge, for which results of modal analysis are available [15, 16].

The introduction section is followed by Section 2 that presents the footbridge
 54 case-study for validation of the proposed approach. Section 3 details how the
 structural system is modelled and how it connects the input excitation to the
 56 output response. Section 4 further details the human-input excitation. Section 5

provides the linkage of this model with measured data, through a statistical
 58 framework that identifies the target modal properties. Sections 6 and 7 highlight
 the main results/discussion and conclusions of this work, respectively.

60 2. Case-study footbridge

This section presents a case-study FRP footbridge and a summary of testing
 62 carried out to infer its dynamic properties. All modal properties, except modal
 masses, were estimated using the instrumented hammer modal testing technique
 64 and free-decay measurements [15], whilst the modal masses were obtained from
 an FE model [16]. These properties will be used as a validation metric for the
 66 approach developed in this work.

2.1. General

68 The footbridge under analysis is a 16.9 m single span beam structure that
 crosses a river valley (Fig. 1(a)). Pultruded fibre-reinforced polymer panels
 70 interlock to form a square 0.78 m wide cross-section (Fig 1(b)). The bridge's
 total mass is approximately 1800 kg. Further details relating to the bridge can
 be found elsewhere [15].

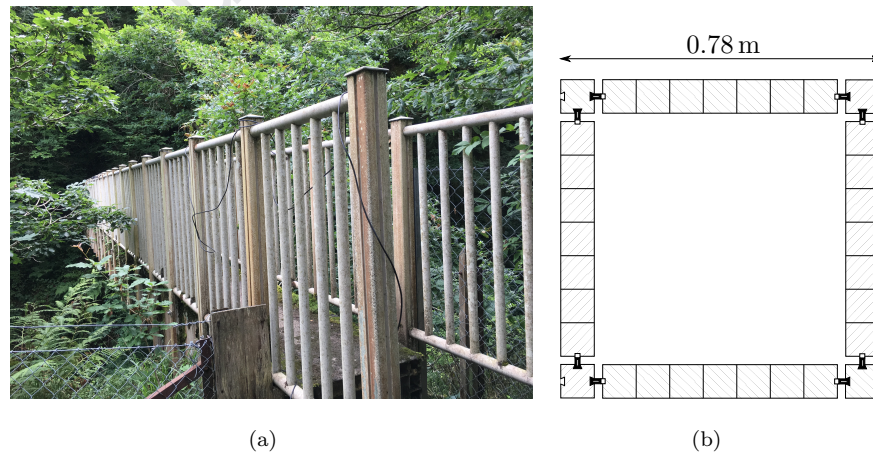


Figure 1: Lively footbridge (a) general view and (b) cross section of individual units that form the footbridge deck.

2.2. Modal testing

74 The current section summarises details about modal tests on the footbridge.
 A detailed description of modal tests can be found in [15] and of FE analysis in [16]. A modal test using an impact hammer was carried out to identify vertical flexural and/or torsional vibration modes in the frequency range
 76 up to 30 Hz. Additionally, the structure was excited by a pedestrian walking at metronome controlled pacing rates from 1.40 Hz to 2.45 Hz in increments of
 78 0.10 Hz or 0.05 Hz – depending of the pacing rate’s proximity to identified natural frequencies. To check repeatability two walks were recorded for each pacing rate. The vibration response was measured at two locations on the deck, and it included recording of the free decay in the response after each crossing.

84 A measurement grid of 18 points (Fig. 2(a)) was used to determine the modal properties. Three roving accelerometers, one of which is shown in Fig. 2(b)
 86 (model QA750 by Honeywell, nominal sensitivity of 1300 mVg^{-1}), were used to simultaneously measure response to hammer impact applied at test point 2 (TP2). After completing one set of measurements at three TPs, the accelerometers were moved to the next three points until the whole grid of 18
 88 TPs was covered, as in a typical roving tri-axial accelerometer test [17]. Im-

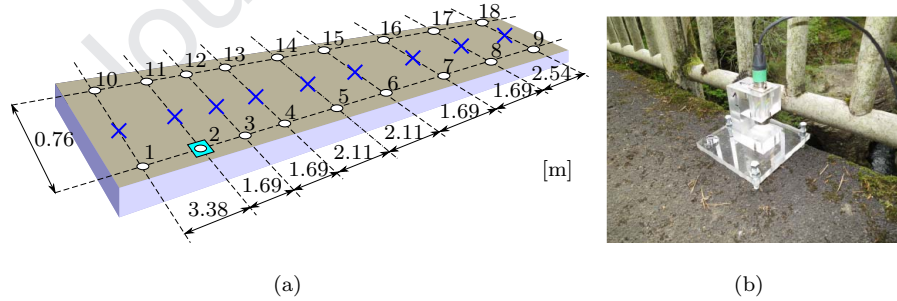


Figure 2: Impact hammer testing (a) measurement grid with circles and square representing response and hammer impact points, respectively, and (b) accelerometer on footbridge deck.

90 pact was applied manually by an experienced operator using an instrumented
 92 sledgehammer (model 5803A by Dytran, nominal sensitivity 0.23 mVN^{-1} and measurement range of 22.2 kN). Data were sampled at 512 Hz. For the walk

94 tests, vertical responses were measured only at TP2 and TP5 at a sampling rate
of 256 Hz. All signals were acquired using a 24-bit, four channel Quattro (by
96 Data Physics) data logger and analyser.

The accelerance FRFs were calculated using six averages. Three flexural
98 vertical modes of vibration at about 4.8 Hz, 15.1 Hz and 28.9 Hz have been
identified and their unity-normalised mode shapes are shown in Fig. 3. By
100 analysing free decay measurements, it was found that the natural frequency
and damping ratio for the fundamental mode are amplitude-dependent, with
102 frequency decreasing from 4.87 Hz to 4.57 Hz and damping ratio increasing from
2.05 % to 2.45 % when vibration amplitude increases up to 1.5 m s^{-2} [15]. The

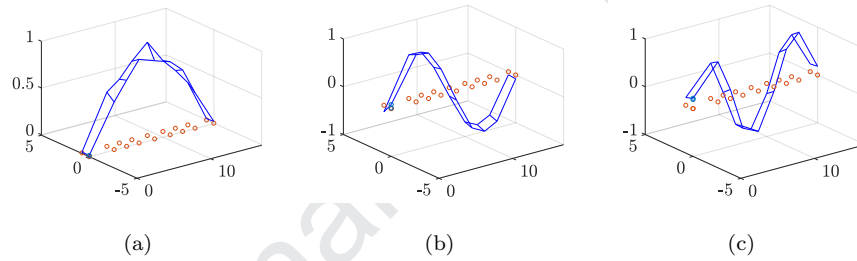


Figure 3: Unity normalised (a) first (b) second and (c) third vertical mode shapes.

104 natural frequencies and damping ratios for the three modes are shown in Table 1.
Finally, due to poor repeatability, the modal masses could not be estimated from
106 the experimental data. This is frequently the case in modal testing, which is the
reason why modal mass information is rarely reported in literature. To overcome
108 this situation an FE model of the bridge has been developed, and it is described
in detail in [16]. The estimated frequencies were 4.9 Hz, 15.8 Hz and 31.4 Hz,
110 and were judged to be sufficiently close to those measured (for estimation of
the modal masses) so not to perform further FE model updating. The resulting
112 modal masses were found to be 862 kg, 907 kg and 839 kg, respectively.

Sample acceleration responses to walking at 1.20 Hz, 2.00 Hz and 2.45 Hz are
114 displayed in Fig 4.

These results constitute the main validation data for the pedestrian-based

f_1	f_2	$f_3(\text{Hz})$	ζ_1	ζ_2	$\zeta_3(\%)$
4.57-4.87	15.1	28.9	2.05-2.45	2.8	2.7

Table 1: Modal properties identified in impact hammer and free decay tests.

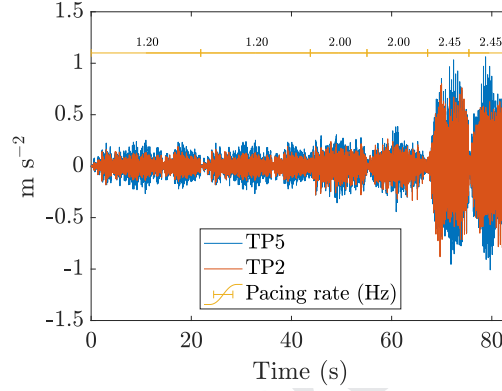


Figure 4: Acceleration responses of footbridge at TP2 and TP5 for three pacing rates at 1.20 Hz, 2.00 Hz and 2.45 Hz.

116 approach presented next.

3. Theoretical framework

118 The pedestrian-based approach is detailed in the following sections and is
illustrated in Fig. 5. The core idea is to match power spectral densities (PSD)
120 of responses induced by a pedestrian on the bridge against theoretical PSDs.
The latter are based on forces obtained using a laboratory treadmill and a
122 probabilistic model of the structure. For the current work there is a eight years
gap between in-field and treadmill experiments. Although this is a significant
124 period of time, the test subject is well experienced in walking tests, has body
mass which hardly changed over time, and has been generating very much the
126 same peak responses when walking over structures similar to the one presented.

The to-be-identified modal properties – natural frequencies, damping ratios
128 and modal masses – are denoted as θ . The framework was implemented with
MATLAB and is available in [18].

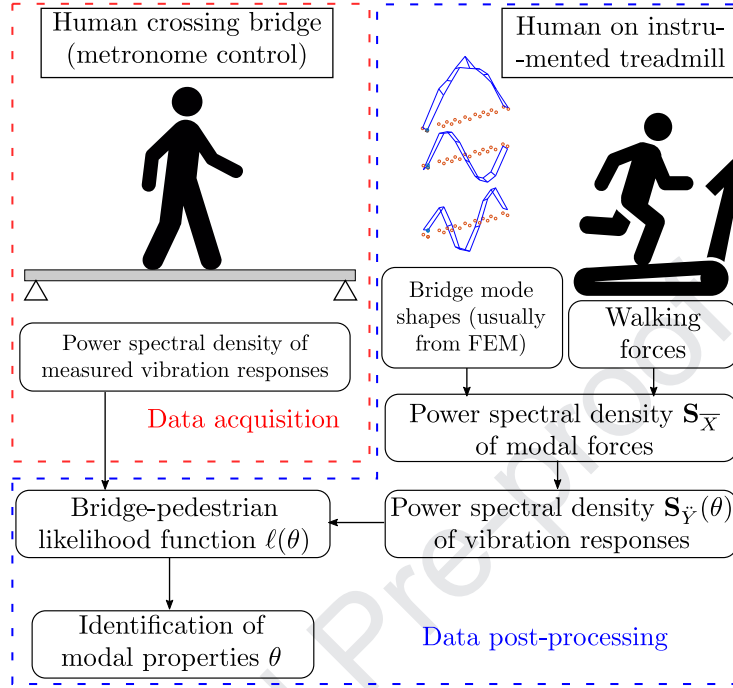


Figure 5: Diagram of spectral pedestrian-based approach.

130 3.1. Equation of motion – time domain

The general equation of motion of a structural system with N_d DOFs can
 132 be written as follows

$$\mathbf{M}\ddot{\mathbf{y}}(t) + \mathbf{C}\dot{\mathbf{y}}(t) + \mathbf{K}\mathbf{y}(t) = \mathbf{x}(t) \quad (1)$$

for a scenario of damped forced vibrations. \mathbf{M} , \mathbf{C} and \mathbf{K} are $N_d \times N_d$ mass,
 134 damping and stiffness matrices, $\ddot{\mathbf{y}}$, $\dot{\mathbf{y}}$, \mathbf{y} and \mathbf{x} are $N_d \times 1$ time-dependent vec-
 tors of acceleration, velocity, displacement and force induced by a pedestrian at
 136 each DOF, respectively. Commonly this equation is transformed into its modal
 equivalent by using the transformation $\mathbf{y}(t)_{N_d \times 1} = \mathbf{\Phi}_{N_d \times n} \mathbf{q}(t)_{n \times 1}$ (for n inde-
 138 pendent vibration modes), with $\mathbf{\Phi} = [\mathbf{\Phi}_1 \mathbf{\Phi}_2 \dots \mathbf{\Phi}_n]$ defined as an $N_d \times n$ mode
 shape matrix. Pre-multiplying Eq. (1) by the transposed mode shape matrix
 140 $\mathbf{\Phi}^T$ results in

$$\mathbf{m}\ddot{\mathbf{q}}(t) + 2\mathbf{m}\zeta\omega_n\dot{\mathbf{q}}(t) + \mathbf{m}\omega_n^2\mathbf{q}(t) = \mathbf{\Phi}^T(t)\mathbf{x}(t) \quad (2)$$

where \mathbf{m} , ζ , ω_n are the n -dimensional diagonal matrices that contain the modal
 142 masses, damping ratios and circular natural frequencies, respectively. The vec-
 tor on the right-hand side represents time-dependent modal forces for given
 144 modes, and \mathbf{q} , $\dot{\mathbf{q}}$, $\ddot{\mathbf{q}}$ are the modal response vectors of displacement, velocity
 and acceleration, respectively. It should be noted that the mode shape matrix
 146 on the RHS of Eq. (2) can be transformed from spatial to time domain using
 $t = l/v$, where l is the longitudinal position of the pedestrian on the bridge
 148 while v is the pedestrian speed (assumed to be constant).

3.2. Frequency response function – frequency domain

150 In this section Eq. (1) is analysed in the frequency domain with the aid of
 the Fourier transform (FT). Taking Eq. (2) as a basis, and applying the FT to
 152 convert it from time into frequency domain, results in

$$\mathbf{m}\ddot{\mathbf{Q}}(\omega) + 2\mathbf{m}\zeta\omega_n\dot{\mathbf{Q}}(\omega) + \mathbf{m}\omega_n^2\mathbf{Q}(\omega) = \bar{\mathbf{X}}(\omega) \quad (3)$$

where $\ddot{\mathbf{Q}}$, $\dot{\mathbf{Q}}$, \mathbf{Q} and $\bar{\mathbf{X}}$ represent the FTs of the modal responses and modal
 154 forces, respectively. In the present work the complex form of the FT is defined
 as

$$X(\omega) = \frac{1}{2\pi} \int_{-\infty}^{\infty} x(t)e^{-i\omega t} dt. \quad (4)$$

156 By definition $\ddot{\mathbf{Q}} = -\omega^2\mathbf{Q}$, $\dot{\mathbf{Q}} = i\omega\mathbf{Q}$ and $\ddot{\mathbf{Q}} = i\omega\dot{\mathbf{Q}}$. The FT of the modal
 acceleration response can be written as:

$$\ddot{\mathbf{Q}}(\omega) = \mathbf{H}(\omega)\bar{\mathbf{X}}(\omega). \quad (5)$$

158 where \mathbf{H} is an n -dimensional diagonal FRF matrix, which is a function of the
 structural modal properties. Accelerance FRF for a single degree of freedom
 160 system is given by

$$H(\omega) = \frac{-\omega^2}{m(-\omega^2 + \omega_n^2 + 2\zeta i\omega_n\omega)}. \quad (6)$$

Now the FT of physical acceleration can be written as

$$\ddot{\mathbf{Y}}(\omega)_{N_d \times 1} = \Phi_{N_d \times n} \ddot{\mathbf{Q}}(\omega)_{n \times 1} = \Phi_{N_d \times n} \mathbf{H}(\omega)_{n \times n} \bar{\mathbf{X}}(\omega)_{n \times 1}. \quad (7)$$

162 Assuming that the response has random fluctuations in it, an N_d -dimensional
 Hermitian PSD matrix at frequency ω can be obtained from the FT of the
 164 response in Eq. (7) as follows

$$\mathbf{S}_{\ddot{\mathbf{y}}}(\omega) = \mathbb{E}[\ddot{\mathbf{Y}}(\omega)\ddot{\mathbf{Y}}(\omega)^H] = \mathbf{\Phi}_{N_d \times n} \mathbf{H}(\omega)_{n \times n} \mathbf{S}_{\overline{\mathbf{X}}}(\omega)^{n \times n} \mathbf{H}(\omega)_{n \times n}^H \mathbf{\Phi}_{n \times N_d}^T, \quad (8)$$

where $\mathbf{S}_{\overline{\mathbf{X}}}$ is an n -dimensional Hermitian PSD matrix of modal forces. This
 166 matrix contains in its diagonal and off-diagonal entries the auto and cross PSD
 between modal forces, respectively. Eq. (8) is the central result of random vibra-
 168 tion theory for a multiple DOF system, and it will be utilised as a data model
 of the bridge-pedestrian system which allows to estimate modal properties.

170 4. Spectral model of the excitation

This section details how the PSD matrix of modal forces in Eq. (8) is ob-
 172 tained. The following text adopts a discretised formulation whereby the PSD of
 modal forces at frequency k , sampled at N points at time interval Δt is denoted
 174 as $\mathbf{S}_{\overline{\mathbf{X}},k}$ ($f_k = k/(N\Delta t)$, $k = 1, \dots, N_f$), where N_f is the frequency bin number
 correspondent to the Nyquist frequency of the discretised signal.

176 The modal force for each mode is calculated by weighting the time history
 of force by the mode shape. Fig. 6(a) shows vertical component of walking
 178 forces by each leg sampled at 200 Hz. The sum of the forces by two feet is then
 calculated and the static weight is removed. The resulting dynamic force is
 180 shown in Fig. 6(b). The force in this example is for walking at 1.20 Hz. The
 modal forces for the three modes from Fig. 3 are shown in Fig. 7.

182 The auto (ASD) and cross (CSD) spectral density terms of the modal forces
 can now be determined. The CSD is a particularly relevant quantity, as it
 184 highlights the correlations between different modal forces.

Assuming now that the modal forces are wide-sense stationary processes,
 186 their PSDs can be estimated by multiplying their DFT with its complex con-
 jugate. Fig. 8 shows an example of the calculated ASD and CSD of the modal
 188 forces. The visible spread of energy around the peaks is characteristic of the

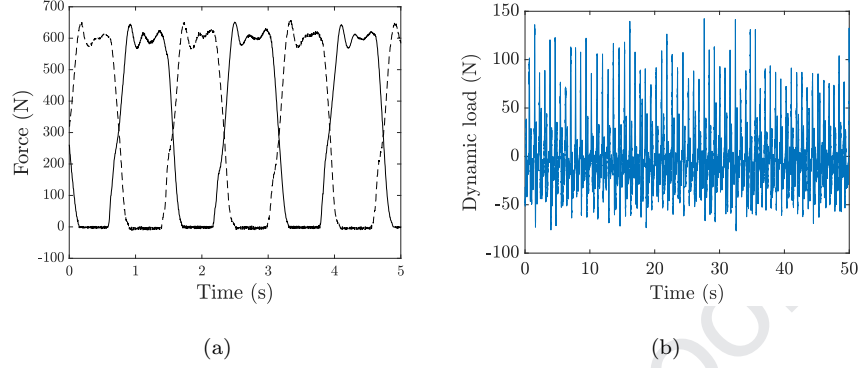


Figure 6: Pedestrian's dynamic load recorded using an instrumented treadmill: (a) individual forces for two feet (solid and dashed lines) and (b) total force with its static component removed.

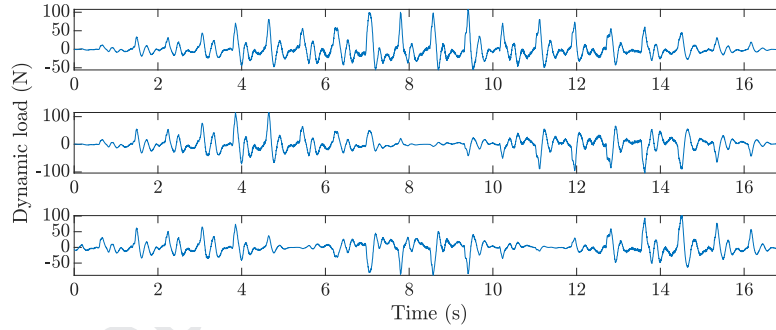


Figure 7: Vertical modal forces for the first three vibration modes walking at 1.20 Hz.

quasi-harmonic human walking nature. In addition to the shown magnitude,
 190 the CSD also contains a phase spectrum (not shown here). Thus, at each fre-
 quency band k of the spectrum a matrix $\mathbf{S}_{\bar{X},k}$ is built from the aforementioned
 192 data and substituted into Eq. (8) to obtain a $\mathbf{S}_{\bar{y},k}$ PSD matrix of simulated
 responses.

194 5. Probabilistic modal identification approach

This section details how the natural frequencies, damping ratios, and modal
 196 masses can be identified using acceleration responses.

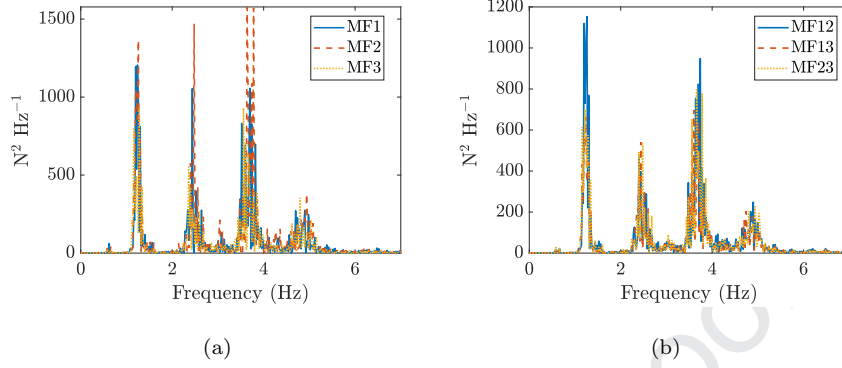


Figure 8: (a) Auto spectral density of modal forces and (b) cross spectral density of modal force pairs. The peaks represent the 1.20 Hz pacing rate and its higher harmonics.

5.1. Scaled discrete Fourier transform of observations

Let us assume that a given stochastic process, in this case the vibration response of the bridge, has N time observations \mathbf{y}_j^e , $j = 0, \dots, N - 1$ at N_d observation channels. The process is dependent on modal properties θ , presented in Section 2.2, as well as on the PSD of the noise at each observation channel. The scaled discrete Fourier transform (DFT) of the observations (frequency $f_k = k/(N\Delta t)$) is given by

$$\mathbf{Y}_k = \sqrt{\frac{2\Delta t}{N}} \sum_{j=0}^{N-1} \mathbf{y}_j^e e^{-i2\pi jk/N} \quad (9)$$

where Δt is the sampling time interval. The scaled DFTs on a selected frequency band represent the core evidence used to identify the modal properties.

5.2. Likelihood function

The likelihood function is a joint probability density function (PDF) of a collection of variables indexed by k $\{\mathbf{Y}_k\}$ for given θ . Assuming long data, $\{\mathbf{Y}_k\}$ are (circularly symmetric) complex Gaussian and independent at different frequencies. This gives

$$p(\{\mathbf{Y}_k\}|\theta) = \prod_k p(\mathbf{Y}_k|\theta) \quad (10)$$

where the product is taken over all frequencies in the selected band with N_f
 212 DFT points, assumed to be large compared to 1 (long data); and

$$p(\mathbf{Y}_k|\theta) = \frac{\pi^{-N_d}}{|\mathbf{S}_k(\theta)|} \exp[-\mathbf{Y}_k^H \mathbf{S}_k(\theta)^{-1} \mathbf{Y}_k] \quad (11)$$

where $\mathbf{S}_k(\theta)$ is a theoretical PSD matrix of data (Hermitian) for a given θ . The
 214 complex Gaussian probability density function (PDF) in Eq. (10) is central to
 the proposed modal analysis framework, as it holds for general stationary data
 216 regardless of the frequency content of contributing activities. The latter affects
 $\mathbf{S}_k(\theta)$ but not the form of the PDF.

218 Next the derivation of $\mathbf{S}_k(\theta)$ is detailed. Within a selected frequency band
 k , the following model is assumed

$$\mathbf{Y}_k = \hat{\mathbf{Y}}_k + \boldsymbol{\varepsilon}_k \quad (12)$$

220 where $\hat{\mathbf{Y}}_k$ and $\boldsymbol{\varepsilon}_k$ represent scaled DFTs of a theoretical structural dynamic
 response and measurement noise, respectively. Similarly, the theoretical PSD of
 222 the data is given by

$$\mathbf{S}_k(\theta) = \mathbb{E}[\hat{\mathbf{Y}}_k \hat{\mathbf{Y}}_k^H | \theta] + \mathbb{E}[\boldsymbol{\varepsilon}_k \boldsymbol{\varepsilon}_k^H | \theta] \quad (13)$$

assuming that the modal forces and the measurement noise are independent.
 224 $\mathbb{E}[\boldsymbol{\varepsilon}_k \boldsymbol{\varepsilon}_k^H | \theta] = \text{diag}(S_e^1, S_e^2, \dots, S_e^{N_d})$, is a diagonal matrix, where each entry S_e^j
 is the PSD of noise in the frequency band (assumed as constant) at the j -th
 226 observation channel. Finally, the PSD of the structural response term can be
 obtained from a modal contribution form, already presented in Eq. (8), and the
 228 DFT of the structural dynamic response $\hat{\mathbf{Y}}_k$ is obtained from Eq. (7).

5.3. Log-likelihood function

230 Mainly for numerical reasons, it is common practice to work with the log-
 likelihood function (LFF) instead of the likelihood in Eq. (11), which can be
 232 expressed as

$$\ell(\theta) = -N_d N_f \ln \pi - \sum_k \ln |\mathbf{S}_k(\theta)| - \sum_k \mathbf{Y}_k^H \mathbf{S}_k(\theta)^{-1} \mathbf{Y}_k. \quad (14)$$

In order to identify the modal properties the LLF is sampled with the Metropolis–
 234 Hastings (MH) algorithm [19]. The samples of θ indicate in which regions of
 the parameter space the bridge-pedestrian model matches available data. In
 236 addition to the likelihood maximum, the samples allow to compute other un-
 certainties, such as the variance of the estimate.

238 The current section is closed with a discussion of some numerical details. In
 order to increase the numerical stability of the matrix inversion in Eq. (14), the
 240 matrix is transformed with a Cholesky decomposition routine. Further details
 of this operation are given in Appendix A.1. Relatively to the MH algorithm,
 242 it is necessary to set a proposal probability distribution (proportional to the
 target distribution), amongst other options which are summarised in Appendix
 244 A.2.

6. Results and discussion

246 6.1. Numerical tests - constant modal properties

A large number of numerical tests have been run to assess the performance
 248 of the pedestrian-based approach. Based on the results from Section 2.2, fixed
 modal parameters were used to generate responses to walking at 12 pacing rates
 250 (see Table 2) using MATLAB. Each force time history measured on the treadmill
 was weighted by the measured shape of each vibration mode (as in the RHS of
 252 Eq. (2)) to determine modal forces for each mode. The modal forces were used
 to calculate the modal responses in each individual vibration mode using the
 254 Fox and Goodwin’s numerical procedure [20]. Then, the mode superposition
 principle was employed to calculate the final acceleration response $\ddot{y}_i(t)$ at a
 256 location i on the deck, given by:

$$\ddot{y}_i(t) = \sum_{k=1}^3 \phi_{i,k} \ddot{q}_k(t), \quad (15)$$

where $\phi_{i,k}$ is the amplitude of the k th mode shape ($k = 1, 2, 3$) at location i ($i =$
 258 $1, \dots, 9$) along the midline of the bridge (crosses in Fig. 2(a)) and $\ddot{q}_k(t)$ is the
 modal response in the k th mode. Three sets were generated for each pacing rate,

260 by dividing the available walking data into three segments, each long enough
for a bridge crossing. This was done to assess the impact of the variability in
262 the force and responses on the accuracy of the system identification.

The parameters were identified by maximising the LLF in Eq. (14) by means
264 of the `fmincon` MATLAB function, rather than sampling it with the MH algo-
rithm; mainly to avoid having to adjust the MH settings for each run. Therefore
266 the identified values correspond to maximum likelihood estimates. It is also im-
portant to stress that a small amount of white noise ($\sigma = 1 \times 10^{-2} \text{ m s}^{-2}$) has
268 been added to the signal, so that matrix $\mathbf{S}_{\bar{X}}$ in Eq. (8) remains semi-positive
definite in regions of low spectral density. Not doing so in a simulated example
can lead to numerical instabilities and inaccurate identifications.

f_1	f_2	$f_3(\text{Hz})$	ζ_1	ζ_2	$\zeta_3(\%)$	m_1	m_2	m_3 (kg)
4.70	15.1	28.9	2.4	2.8	2.7	862	907	839

Pacing rates (Hz)											
1.40	1.55	1.60	1.75	1.80	1.88	2.00	2.05	2.20	2.25	2.30	2.45

Table 2: Fixed modal parameters and pacing rates used for response generation.

270 The identified natural frequencies, damping ratios and modal masses are
shown in Figs. 9 and 10. The modal properties are identified within a small error
272 margin except for the first damping ratio, which ranges from 1.5 % to 3.0 %. The
other two damping ratios are less scattered and have a smaller relative error (up
274 to 10.7 % for ζ_2 and 18.5 % for ζ_3). Squares, crosses and circles in Fig. 9 and 10
represent results for the first, two and all three runs, respectively.

For the identification of modal masses, Fig. 10, the method performs well
278 across all vibration modes, attaining the best results in the central region of
pacing rates.

280 The relative error is shown in Table 3. Each row of the table corresponds to
an error of a cumulative average of the values shown in the above plots, i.e., for
282 one, two and all three runs across the bridge. The averages were calculated con-
sidering all pacing rates. It can be seen that the errors for natural frequencies

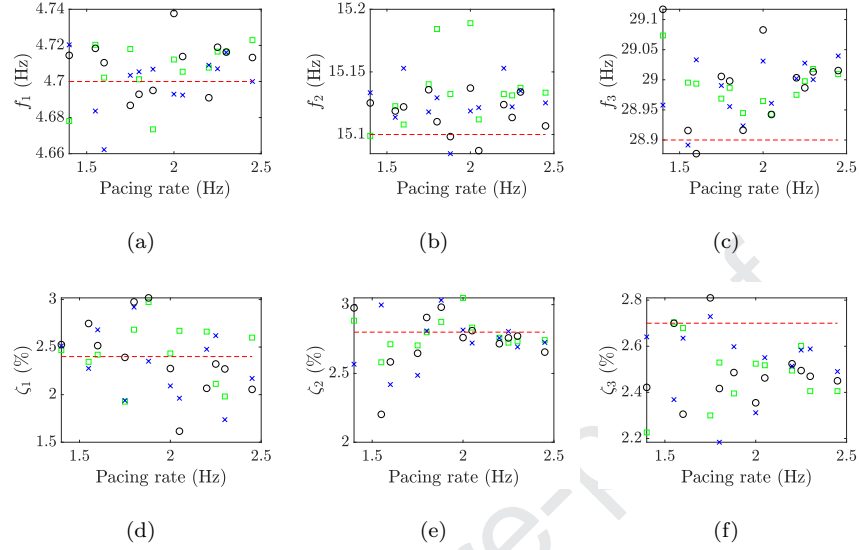


Figure 9: Identified (a-c) natural frequencies and (d-f) damping ratios at several pacing rates for first (squares), second (crosses) and third runs (circles), and their true value (horizontal dashed line).

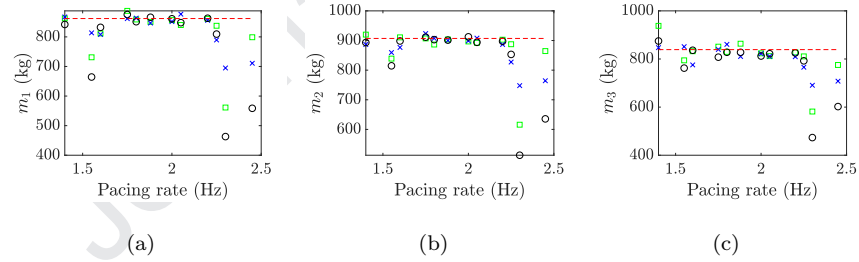


Figure 10: Identified (a-c) modal masses at several pacing rates for first (squares), second (crosses) and third runs (circles), and their true value (horizontal dashed line).

284 are negligible and the largest absolute value for the error is about 8% for ζ_3 .
 There is no significant error improvement beyond a single run across the bridge.
 286 This error is a consequence of treating the measured signals as wide sense stationary in Eq. (8). The error can be said to be sufficiently small for practical
 288 purposes. Note that for longer bridges this error would further decrease.

Averages	f_1	f_2	f_3	ζ_1	ζ_2	ζ_3	m_1	m_2	m_3
1	0.13	0.23	0.30	1.63	-0.61	-8.07	-5.66	-4.20	-3.26
2	0.06	0.20	0.30	-1.02	-1.45	-7.44	-5.26	-4.38	-3.99
3	0.10	0.17	0.30	-0.71	-1.79	-7.53	-6.76	-5.55	-5.32

Table 3: Relative error (%) of identifications for an increasing number of runs averages.

Parameter		α_0	α_1	α_2	α_3	α_4	α_5
f_1	Hz	4.872	-0.4958	0.3387	-0.1227	0.02112	-0.001364
ζ_1	%	2.073	1.167	-1.368	0.6789	-0.1526	0.01235

Table 4: Polynomial regression coefficients of amplitude-dependent modal properties.

6.2. Numerical tests - amplitude-dependent modal properties

290 This section highlights a more challenging simulated example of modal identification with amplitude-dependent modal properties. In an attempt to emulate
292 the real behaviour of the footbridge, the first natural frequency and damping ratio were modelled as amplitude-dependent. Specifically, they were modelled
294 as 5th order polynomial functions of the peak acceleration (see Table 4) as obtained fitting free-decay data. The equation of motion was solved by using Fox
296 and Goodwin's numerical procedure [20]. Since the damping ratio and natural frequency of the first mode are functions of vibration amplitude (Table 4), their
298 values for simulating the response in the next vibration cycle are taken using maximum absolute values from the previous cycle. When simulating response
300 in the first cycle, the values of 4.872 Hz and 2.073 % were used (free coefficients in Table 4). All the other modal parameters were kept constant, as defined in
302 the previous section.

The identified natural frequencies are shown in Fig. 11. The shaded area
304 in Fig. 11(a) shows an actual range of natural frequencies that corresponds to the vibration amplitude range. The identified natural frequency lies within the
306 area, i.e., the method approximates the amplitude-dependent natural frequency with a constant value from within the actual range. Similarly to the previous

section, the other natural frequencies are identified within a small error margin (up to 1.99 % for f_2 and 1.38 % for f_3).

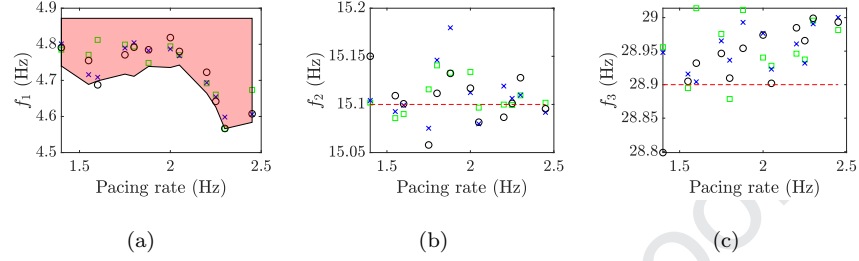


Figure 11: Identified (a–c) natural frequencies at several pacing rates for first (squares), second (crosses) and third runs (circles) and their true values (shaded area and horizontal dashed lines).

Fig. 12 shows the identified damping ratios and modal masses. Similarly to the previous section, modal masses are identified in a consistent manner across all three vibration modes, whereas the first damping ratio has a larger variability across pacing rates than the other two ratios. Compared with the results in the previous section the estimate of damping ratios identification have worsened, which suggests that identification of these modal properties is susceptible to nonlinear effects. For the modal masses, Figs. 12(d)12(e)12(f) indicate a reliable estimation within a central band, from 1.75 Hz to 2.20 Hz of the pacing rates, while the results are more erroneous for pacing rates at 1.55 Hz and 2.30 Hz, whose third and second harmonic, respectively, are close to the natural frequency of the first mode. In the authors' opinion, the reason is that close peaks are present in the spectrum in these tests and the identification becomes sensitive to frequency resolution of the signal, which is particularly coarse in case of faster walking (when the time domain signal is shorter).

As in the previous section, the relative error of the identifications is shown in Table 5. For the amplitude-dependent modal properties, the “true” value was considered as the mid-value of the lines that outline the shaded areas in Figs. 11(a) and 12(a). For the current example the damping ratios have the largest observed errors, and once again, there is no considerable difference be-

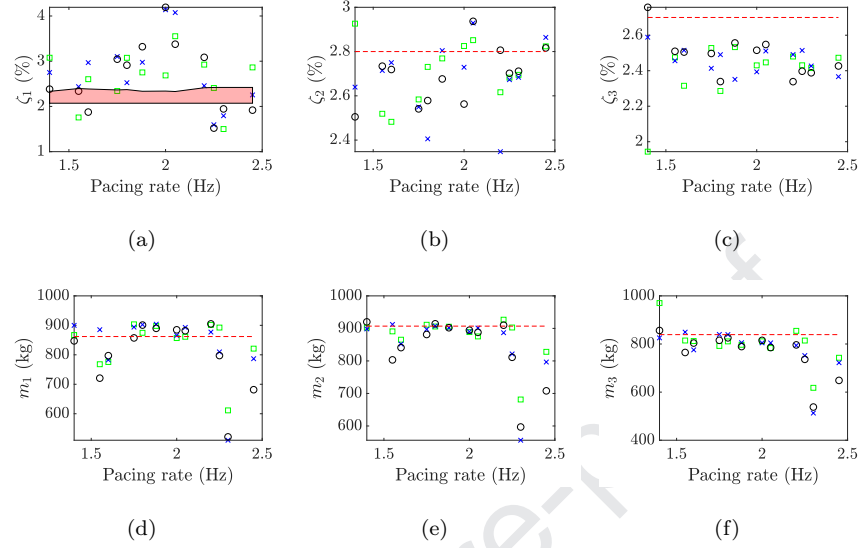


Figure 12: Identified (a-c) damping ratios and (d-f) modal masses at several pacing rates for first (squares), second (crosses) and third runs (circles), and their true value (shaded areas and horizontal dashed lines).

tween the average error with one or more runs across the bridge.

Averages	f_1	f_2	f_3	ζ_1	ζ_2	ζ_3	m_1	m_2	m_3
1	-0.82	0.06	0.19	18.16	-3.26	-11.24	-3.03	-3.67	-4.44
2	-0.96	0.06	0.18	21.04	-3.87	-10.06	-3.12	-4.88	-5.91
3	-1.00	0.05	0.17	20.55	-3.89	-9.41	-4.20	-5.75	-6.90

Table 5: Relative error (%) of identifications for an increasing number of runs averages.

330 6.3. Measurements on the footbridge

In this section acceleration data measured at TP2 and TP5 on the actual
 332 footbridge (Fig. 4) are used for validation of the pedestrian-based approach.

Results will be compared against measured modal properties reported in Sec-
 334 tion 2.2.

The MH algorithm was fine-tuned to obtain the distribution of the modal
 336 properties with a burn-in period of 6000 samples, followed by a total of 10 000

samples. Since the data in Sections 2.2 and 4 were sampled at 256 Hz and
 200 Hz, respectively, the former has been resampled down to 200 Hz, so that the
 theoretical and experimental PSD responses have the same frequency resolution.
 The results related to walking at 1.40 Hz, 1.55 Hz, 1.60 Hz, 1.75 Hz, 1.80 Hz,
 1.88 Hz, 2.00 Hz, 2.05 Hz, 2.25 Hz, 2.30 Hz and 2.45 Hz are presented.

One of the differences relative to the previous numerical examples is that
 the measured vibration response is caused by a force generated by a person
 walking over the bridge that inevitably differs from the treadmill force used in
 the analysis [21, 22].

The estimated natural frequencies and damping ratios are shown in Fig. 13.
 The error bars represent a 99.7% confidence interval of the estimate computed
 from the MH samples, and the squares and crosses represent the identified mean
 value for the first and second run, respectively. The identifications of the second

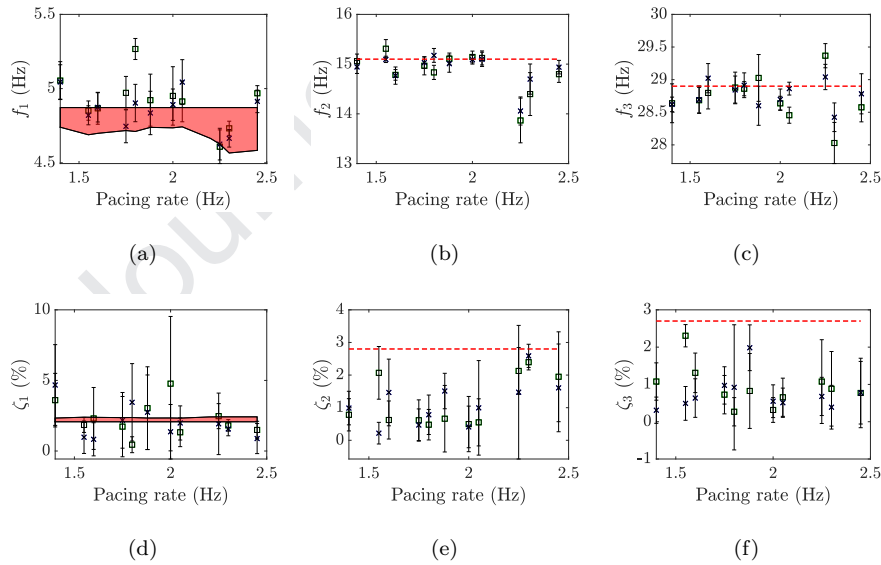


Figure 13: Identified (a-c) natural frequencies and (d-f) damping ratios, mean values (circles) and 99.7% confidence intervals (error bars) for different pacing rates. The reference values are the shaded area and horizontal dashed lines.

and third damping ratio are biased because of their sensitivity to nonlinearities
 and the now present intra-subject variability. If the walking frequency in Fig. 8

is slightly offset from the pedestrian's step rate on the bridge, there is an offset between the harmonics of these two types of excitation, which would be increasingly larger the higher the harmonic is. Thus, higher frequencies are more affected by intra-subject variability than lower frequencies, which agrees with the presented results for the second/third and the first damping ratio, respectively.

To further minimise errors, the time lag between treadmill and in-field recordings should also be as small as possible, especially if the test subject is inexperienced with walking tests.

Lastly, the modal masses identification is shown in Fig. 14. The error has increased in comparison with the numerical examples, but it is still within 30 % mark achieved when using other more elaborate test setups. The increase in this error is partially due to uncertainty of the actual modal masses associated with estimating them using the FE model.

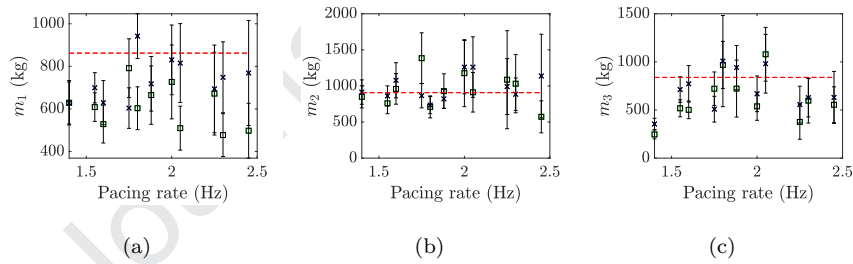


Figure 14: Identified (a–c) modal masses mean values (circles) and 99.7 % confidence intervals (error bars) at several pacing rates. Their reference values are the horizontal dashed lines.

The relative errors are presented in Table 6. The maximum absolute value of the error is up to 3 %, 69 % and 22 % for natural frequencies, damping ratios and modal masses, respectively. The main difference comparatively to the numerical examples is the more pronounced bias of the identified second and third damping ratios.

The errors for natural frequencies and modal masses are sufficiently small to be competitive against other types of tests (shaker, impact hammer and ambient), whilst the errors in damping ratios can be large. Overall, simplicity

Averages	f_1	f_2	f_3	ζ_1	ζ_2	ζ_3	m_1	m_2	m_3
1	2.94	-1.62	-0.61	-1.79	-58.61	-65.61	-29.25	3.94	-26.06
2	2.23	-1.47	-0.52	-6.28	-58.99	-68.97	-22.03	6.15	-20.97

Table 6: Relative error (%) of average of identifications for field measurements.

in data collection using the proposed method and promising nature of the results suggest that the method has potential to be used in system identification and it is worth investigating and improving further in future research.

7. Conclusions

An approach, with potential to identify modal properties using a pedestrian excitation, has been developed and applied to a lightweight FRP footbridge. The approach was validated against both numerical and field data.

The methodology was found to provide reliable modal properties estimates, with the exception of damping ratios when considering a structure with amplitude-dependent behaviour. Generally, the best results are obtained with pacing rates that are not close to the structure's resonant frequency. Additionally, preliminary numerical tests (not presented here) indicate that the approach can be applied to heavier and less responsive bridges with similar error margins. Therefore, future work is required to explore the extents of the methodology.

The proposed model can be further developed by replacing the treadmill-based pedestrian walking forces by a probabilistic model of an overground walker; or by enhancing the proposed statistical model to account for model bias and human-structure interaction effects; and reimplementing the approach on the basis of a structure with amplitude-dependent behaviour to improve the identification of damping ratios.

Nevertheless, the reported errors for natural frequencies and modal masses are sufficiently small comparatively to the typically used tests. Thus, the pedestrian-based approach's reliability, cost-effectiveness and simplicity further justify future developments.

398 Acknowledgements

The authors would like to thank the anonymous reviewers/editor and Julia
 400 Dinan for feedback on the manuscript. The research in this paper was partially
 supported by the UK Engineering and Physical Sciences Research Council (grant
 402 number EP/M021505/1 Characterising dynamic performance of fibre reinforced
 polymer structures for resilience and sustainability).

404 Appendix A. Computational aspects

Appendix A.1. Cholesky decomposition

406 This section details some of the computational aspects of the proposed frame-
 work. Although matrix $S_k(\theta)$ in Eq. (11) is not expected to be very large – its
 408 dimension corresponds to the number of DOF – it can become ill-conditioned.
 Furthermore, determining its inverse and determinant can be computationally
 410 costly. The current approach exploits the fact that it is an Hermitian semi-
 positive definite matrix, and therefore, can be factorised with the Cholesky
 412 decomposition as

$$\mathbf{S}_k(\theta) = \mathbf{C}(\theta)\mathbf{C}(\theta)^H, \quad (\text{A.1})$$

with $\mathbf{C}(\theta)$ as a lower triangular matrix. This transformation allows an orthog-
 414 onal transformation from the generalised to ordinary least squares solution of
 the overdetermined system to be performed:

$$\mathbf{C}_k(\theta)\tilde{\mathbf{Y}}_k = \mathbf{Y}_k. \quad (\text{A.2})$$

416 Having presented the factorisation, the original dataset \mathbf{Y} and the PSD matrix
 of the theoretical model can now be very simply replaced by their transformed
 418 equivalents to simplify the likelihood functions shown in the original formula-
 tion. Thus, Eq. (11) becomes

$$p(\mathbf{Y}_k|\theta) = \frac{\pi^{-N_d}}{|\mathbf{C}_k(\theta)|^2} \exp[-\tilde{\mathbf{Y}}_k^H \tilde{\mathbf{Y}}_k] \quad (\text{A.3})$$

420 and Eq. (14) becomes

$$\ell(\theta) = -N_d N_f \ln \pi - 2 \sum_k \ln |\mathbf{C}_k(\theta)| - \sum_k \tilde{\mathbf{Y}}_k^H \tilde{\mathbf{Y}}_k. \quad (\text{A.4})$$

Appendix A.2. Details of the Metropolis–Hastings algorithm

422 The Metropolis–Hastings algorithm belongs to the class of Markov Chain
 Monte Carlo (MCMC) algorithms, that approximate a target multi-dimensional
 424 probability distribution with a large number of samples. The algorithm has to be
 fine-tuned so that the obtained samples reflect the target distribution faithfully,
 426 i.e. regions of low probability density are visited less frequently by the sampling
 routine than regions of high density. In the context of the current work, each
 428 dimension of the sampled target distribution corresponds to one of the modal
 properties and noise PSD.

430 An important aspect of the whole procedure is the correlation between iden-
 tified modal parameters, which has to be as low as possible. An indicator of the
 432 correlation between modal properties marginal PDFs is the correlation matrix,
 defined as

$$\mathbf{R}(\theta) = (\text{diag}(\mathbf{\Sigma}))^{-\frac{1}{2}} \mathbf{\Sigma} (\text{diag}(\mathbf{\Sigma}))^{-\frac{1}{2}}, \quad (\text{A.5})$$

434 where $\mathbf{\Sigma}$ is the modal parameters covariance matrix, and $\text{diag}(\mathbf{\Sigma})$ is a diagonal
 matrix of the elements of $\mathbf{\Sigma}$. The entries of the correlation matrix represent
 436 the Pearson coefficients, i.e. the linear dependency between the parameters,
 with a $-1, 0, 1$ representing a perfectly negative, lack of, or perfectly positive
 438 correlation between parameters, respectively.

Furthermore, three other options have to be set:

- 440 1. a proposal distribution that guides where the Markov chain will move at
 each iterative step;
- 442 2. a random generator routine for each of the sampled parameters;
3. the number of burn-in samples, to skip low probability density regions
 444 during the initial steps of the chain;

In the current work, a uniform distribution g has been adopted as the proposal
 446 distribution, within an interval $[-\delta; \delta]$ as follows

$$g(\theta'|\theta) = \begin{cases} \frac{1}{2\delta} & \text{for } -\delta \leq \theta - \theta' \leq \delta \\ 0 & \text{for } \theta - \theta' < -\delta \text{ or } \theta - \theta' > \delta \end{cases} \quad (\text{A.6})$$

where θ and θ' correspond to a current and newly generated sample of the modal properties, respectively. The random sample generator was also assumed as a uniform sampling grid, centred at θ and within a $\pm\delta$ interval. The burn-in period was set as 2000 for a total amount of 10 000 samples of a symmetric target distribution.

The factor with more influence in the correlation of the samples and convergence speed of the MH algorithm is the proposal distribution's jumping width vector, δ . The jumping width must be large enough so that the modal parameters are not excessively correlated. In a scenario when there is a trade-off between a reasonable acceptance rate and uncorrelated modal parameters, it is necessary to increase the total amount of samples and involved computational effort.

References

- [1] J. Brownjohn, P. Reynolds, S.-K. Au, D. Hester, M. Bocian, Experimental modal analysis of civil structures: State of the art, in: SHMII – 7th International Conference on Structural Health Monitoring of Intelligent Infrastructure, 2015.
- [2] E. Caetano, Á. Cunha, Modal Testing of the Vasco daGama Bridge, Portugal, in: C. Boller, F.-K. Chang, Y. Fujino (Eds.), Encyclopedia of Structural Health Monitoring, John Wiley & Sons, Ltd, Chichester, UK, 2008. doi:[10.1002/9780470061626.shm168](https://doi.org/10.1002/9780470061626.shm168).
- [3] F. Magalhães, E. Caetano, Á. Cunha, O. Flaman, G. Grillaud, Ambient and free vibration tests of the Millau Viaduct: Evaluation of alternative processing strategies, Engineering Structures 45 (2012) 372–84.
- [4] S.-K. Au, Uncertainty law in ambient modal identification—Part I: Theory, Mechanical Systems and Signal Processing 48 (2014) 15 – 33.
- [5] S.-K. Au, Uncertainty law in ambient modal identification—Part II: Im-

- 474 plication and field verification, *Mechanical Systems and Signal Processing*
48 (2014) 34 – 48.
- 476 [6] C. W. Kim, M. Kawatani, J. Hao, Modal parameter identification of short
span bridges under a moving vehicle by means of multivariate AR model,
478 *Structure and Infrastructure Engineering* 8 (2012) 459–72.
- [7] P. Reynolds, A. Pavic, Impulse Hammer Versus Shaker Excitation for the
480 Modal Testing of Building Floors, *Experimental Techniques* 24 (2000) 39–
44.
- 482 [8] R. R. Craig, A. Kurdila, R. R. Craig, *Fundamentals of Structural Dynam-*
ics, 2nd ed ed., John Wiley, Hoboken, N.J, 2006. OCLC: ocm61247316.
- 484 [9] S.-K. Au, *Operational Modal Analysis*, Springer Berlin Heidelberg, New
York, NY, 2017.
- 486 [10] J. Brownjohn, A. Pavic, Experimental methods for estimating modal mass
in footbridges using human-induced dynamic excitation, *Engineering Struc-*
488 *tures* 29 (2007) 2833–43.
- [11] J. M. W. Brownjohn, M. Bocian, D. Hester, A. Quattrone, W. Hudson,
490 D. Moore, S. Goh, M. S. Lim, Footbridge system identification using wire-
less inertial measurement units for force and response measurements, *Jour-*
492 *nal of Sound and Vibration* 384 (2016) 339–55.
- [12] G. Piccardo, F. Tubino, Equivalent spectral model and maximum dynamic
494 response for the serviceability analysis of footbridges, *Engineering Struc-*
tures 40 (2012) 445–56.
- 496 [13] K. Lievens, G. Lombaert, K. Van Nimmen, G. De Roeck, P. Van den
Broeck, Robust vibration serviceability assessment of footbridges subjected
498 to pedestrian excitation: Strategy and applications, *Engineering Structures*
171 (2018) 236–46.

- [14] E. Shahabpoor, A. Pavic, V. Racic, Identification of walking human model using agent-based modelling, *Mechanical Systems and Signal Processing* 103 (2018) 352–67.
- [15] X. Wei, J. Russell, S. Živanović, J. Toby Mottram, Measured dynamic properties for FRP footbridges and their critical comparison against structures made of conventional construction materials, *Composite Structures* 223 (2019) 110956.
- [16] X. Wei, H.-P. Wan, J. Russell, S. Živanović, X. He, Influence of mechanical uncertainties on dynamic responses of a full-scale all-FRP footbridge, *Composite Structures* 223 (2019) 110964.
- [17] B. J. Schwarz, M. H. Richardson, Experimental modal analysis, in: *In Proceedings of CSI Reliability Week*, 1999.
- [18] A. Jesus, Data for: A spectral pedestrian-based approach for modal identification, 2019. doi:[10.17632/cj7353cc9j.1](https://doi.org/10.17632/cj7353cc9j.1).
- [19] I. Yildirim, Bayesian Inference: Metropolis-Hastings Sampling, Dept. of Brain and Cognitive Sciences, Univ. of Rochester, Rochester, NY (2012).
- [20] L. Fox, E. T. Goodwin, Some new methods for the numerical integration of ordinary differential equations, *Mathematical Proceedings of the Cambridge Philosophical Society* 45 (1949) 373–88.
- [21] J. Chen, J. Wang, J. M. W. Brownjohn, Power Spectral-Density Model for Pedestrian Walking Load, *Journal of Structural Engineering* 145 (2019) 04018239.
- [22] M. García-Diéguez, J. Zapico-Valle, Statistical modelling of spatiotemporal variability of overground walking, *Mechanical Systems and Signal Processing* 129 (2019) 186–200.

Author contribution statements

A. J and S. Z conceived the presented idea. A. J. developed the theory and performed the computations. S.Z. provided the simulated and experimental data. A.A. verified the numerical methods developed by A.J. A.J. and S.Z. discussed the results and contributed to the final manuscript.

Declaration of interests

X The authors declare that they have no known competing financial interests or personal relationships that could have appeared to influence the work reported in this paper.

☐ The authors declare the following financial interests/personal relationships which may be considered as potential competing interests: